RSC Advances

This article can be cited before page numbers have been issued, to do this please use: Y. Yang, J. Xiao, H. Wei, L. Zhu, D. Li, Y. Luo, H. Wu and Q. Meng, *RSC Adv.*, 2014, DOI: 10.1039/C4RA09519G.

ROYAL SOCIETY OF CHEMISTRY

www.rsc.org/advances

View Article Online
DOI: 10.1039/C4RA09519G

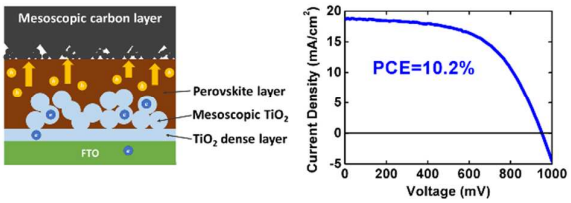

The graphite/carbon black composite counter electrode can achieve an efficiency up to 10.2% for perovskite solar cells.

Dynamic Article Links ▶ View Article Online
DOI: 10.1039/C4RA09519G

Cite this: DOI: 10.1039/c0xx00000x

www.rsc.org/xxxxxx

ARTICLE TYPE

All-carbon counter electrode for highly efficient hole-conductor-free organo-metal perovskite solar cells

Yueyong Yang [a], Junyan Xiao [a], Huiyun Wei [a], Lifeng Zhu [a], Dongmei Li [a], Yanhong Luo [a], Huijue Wu [a] and Qingbo Meng [a]*

Received (in XXX, XXX) Xth XXXXXXXXX 20XX, Accepted Xth XXXXXXXXX 20XX
DOI: 10.1039/b000000x

An all-carbon counter electrode has been fabricated for hole-conductor-free organo-metal perovskite heterojunction thin-film solar cells by a simple and low-temperature process. The counter electrode consisted of two parts: a mesoscopic carbon layer for the good contact with the perovskite layer, and a piece of industrial flexible graphite sheet as the conducting electrode. Several types of carbon materials were employed in the counter electrodes and tested. By electrochemical impedance study, it is found that the contact between counter electrode and perovskite layer has significant influence on the charge transport properties of the cells. A power conversion efficiency up to 10.2% has been achieved by hole-conductor-free mesoscopic $CH_3NH_3PbI_3/TiO_2$ heterojunction solar cells with the counter electrode containing the composition of graphite and carbon black, which inspires a new promising route towards low-cost and large-scale commercialization of perovskite solar cells.

Introduction

Recently, organo-metal perovskite solar cells have attracted great attention around the globe. In the past few years, a lot of effort has been devoted to investigating different types of perovskite solar cells and improving the cell performance[1-3]. Till now, several types of perovskite solar cells can exhibit high power conversion efficiencies (PCE) over 10%, and even a certified record PCE of 17.9% has been achieved[4-8]. Compared with traditional solar cells, the perovskite solar cells can achieve high efficiency with low-cost and easy fabrication process. Especially for the hole-conductor-free perovskite solar cells, the use of expensive organic/polymeric hole-transporting materials is avoided, which can significantly reduce materials costs[9, 10].

Counter electrode (CE) plays a very important part in solar cells[11-13]. For most organo-metal perovskite solar cells reported so far, Au is the most efficient and widely used CE material. However, Au is expensive and increases the overall manufacturing cost of the perovskite solar cells. Cheaper metals like Ag work well in perovskite cells with HTM layer, but they cannot stay stable in HTM-free perovskite cells[14]. Considering the fierce competition of the global photovoltaic market, to make this type of solar cells competitive commercial products, inexpensive CEs with acceptable performance need to be developed.

Carbon materials are low-cost and highly available industrial materials, which have been applied in highly efficient CEs of dye-sensitized solar cells [15-18] and quantum dot-sensitized solar cells [19]. The approximate 5.0 eV work function makes carbon the ideal CE material for perovskite solar cells[20]. Recently, several types of carbon CEs have been applied successfully in perovskite solar cells[20-22], suggesting that carbon materials are prospective candidates of CE materials for hole-conductor-free perovskite solar cells. However, some issues of the carbon CE still exist: (1) currently most fabrication methods were relatively complicated, which induced additional high-temperature procedures or redeveloped optimized methods for photoelectrodes, and (2) the key factors influencing the performance of CEs was not clear enough. Therefore, it is of significant importance to develop new carbon CEs for perovskite solar cells and further study its mechanism.

Here, we report a simple and low-temperature processable all-carbon flexible CE for highly efficient perovskite solar cells. Industrial flexible graphite sheet was used as the conducting electrode and a mesoscopic carbon layer was used for the good contact with the perovskite layer. A two-step process was employed to fabricate the CEs. In this process, no insulating space layer or additional high-temperature sintering procedure were needed. This carbon CE can adapt to any hole-conductor-free perovskite solar cells without changing the current process of fabricating photoelectrodes. By the optimization of CE components, a PCE of 10.2% has been achieved by hole-conductor-free mesoscopic $CH_3NH_3PbI_3/TiO_2$ heterojunction solar cells. Moreover, the key factors influencing the performance of carbon CEs have been investigated, which can help exploit the potential improvement of perovskite solar cells with carbon CEs in the future.

Results and discussion

A total of five types of carbon CEs were fabricated and incorporated in HTM-free perovskite solar cells by a simple process (Fig. 1). In all of these CEs, butadiene-styrene rubber

View Article Online
DOI: 10.1039/C4RA09519G

and ethyl cellulose acted as the binder in the carbon film, and their weight ratios were both 2.5%. The total weight ratio of carbon materials was 95%. CE A, B and C contained three types of pure graphite with different sizes. CE D contained the composition of the smallest graphite and carbon black (CB). The weight ratio of graphite and CB was 75% and 20%, respectively. CE E contains the pure CB. The mesoscopic carbon films were formed by screen printing. For CE A, B, C and D, the carbon films were all even and uniform. However, for CE E, the film cracked into many small pieces during the drying process, which made it impossible for CE E to be applied as the practical CE in cells.

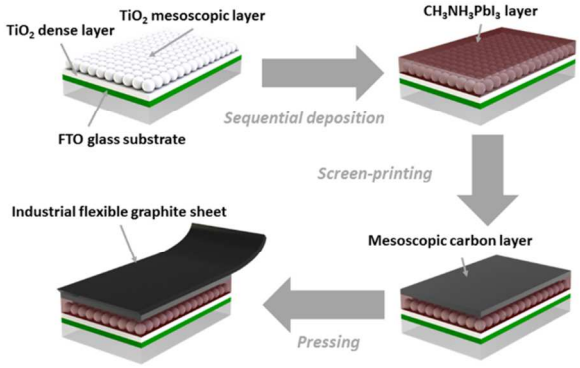

Fig.1 Scheme of the fabrication process of all-carbon flexible CE based HTM-free perovskite solar cells.

The surface morphology of CE A, B, C and D are shown in Fig.2. The accumulation structure of graphite flakes can be clearly seen in the SEM images. Estimated from the SEM images, the sizes of graphite flakes in CE A, B and C are around 20 μm, 3 μm and 1 μm, respectively. In CE D, a composite structure of graphite and CB can be observed. The size of CB particles is less than 100 nm. The small CB particles fill in the interspace between the graphite flakes, and are held tightly on the graphite framework by the binder. The SEM cross-section image of the HTM-free perovskite solar cell with CE D is shown in Fig.2 (g) and (h). The thickness of the FTO layer, mesoscopic TiO_2 layer, perovskite capping layer and mesoscopic carbon layer is 359 nm, 449 nm, 359 nm and 23 μm, respectively.

The conductivity of the mesoscopic carbon films was measured. These films were first coated on insulated glass substrate by screen-printing technique. A four-point probe resistivity measurement system was employed to measure the sheet resistance of the carbon films. The thickness of the carbon films was measured by a profiler. The final results of resistivity are shown in Table 1. The resistivity of CE sample A, B, C and D is 0.127, 0.677, 0.941 and 0.802 Ω cm, respectively. CEs that contain larger graphite flakes exhibit better conductivity. The differences in the conductivity of the CE A, B and C are probably caused by the different densities of interfaces between carbon flakes. For CEs with smaller graphite flakes, there are more interfaces between different graphite flakes, which contributes higher contact resistance to the mesoscopic carbon film. On the other hand, the graphite/CB composite CE (CE D) shows quite closed resistivity compared with CE C, suggesting that in graphite/CB composite CE, the graphite framework is still the major pathway of charge transportation in the composite carbon film. Although the small CB particles create more interfaces, they do not influence much on the overall conductivity of the CE. In our CE, the thickness of the mesoscopic carbon films was approximately 20 μm. As the flexible graphite sheet, whose sheet resistance is only 4.2×10^{-2} Ω/□, is used as the conducting electrode, the total contribution of the carbon CE to the series resistance of the cell is quite small.

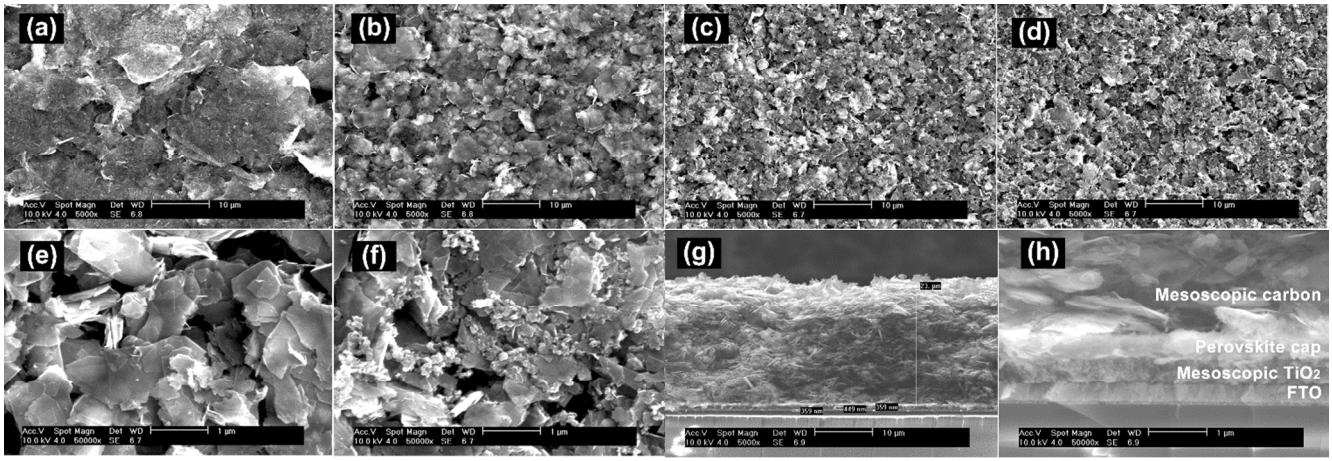

Fig. 2 Top view SEM images of different CE samples. (a), (b), (c) and (d) show the surface image of CE A, B, C, and D, respectively. (e) Magnified image of CE C. (f) Magnified image of CE D. (g) SEM cross-section image of the HTM-free perovskite solar cell with CE D. The industrial flexible graphite sheet has not been clipped on the mesoscopic carbon layer yet. (h) Magnified image of (g).

View Article Online
DOI: 10.1039/C4RA09519G

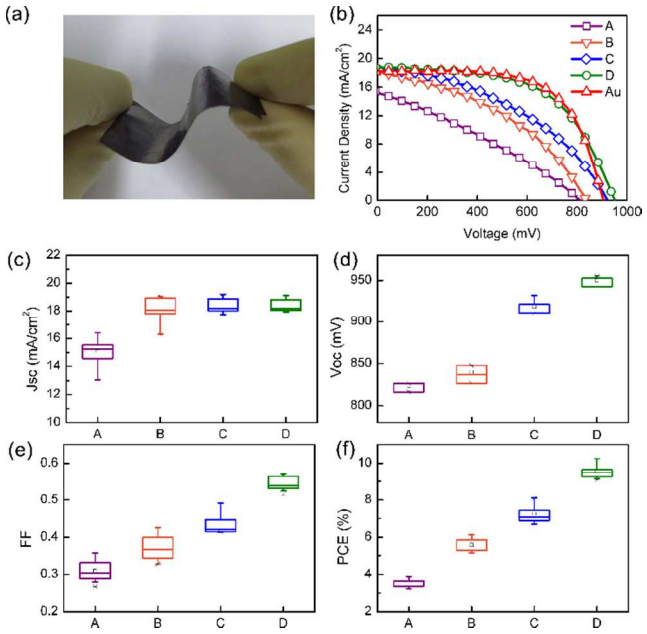

Fig.3 (a) Photo of a typical flexible carbon CE. (b) The *J-V* characteristics of HTM-free $CH_3NH_3PbI_3/TiO_2$ heterojunction solar cells with different CEs. (c), (d), (e) and (f) are the box charts exhibiting the statistical features of short-circuit current density (J_{SC}), open-circuit voltage (V_{OC}), fill factor (FF) and power conversion efficiency (PCE) of all the cells with carbon CEs tested.

$J-V$ curves of the representatives of these cells tested under AM 1.5 100 mW/cm^2 are shown in Fig. 3(b). Detailed data are presented in Table 2. Fig. 3(c), (d), (e) and (f) are the box charts exhibiting the statistical features of short-circuit current density (J_{SC}), open-circuit voltage (V_{OC}), fill factor (FF) and PCE of all the cells with carbon CEs tested. Cells with CE A, which contain the largest graphite flakes, show the poorest performance. The fill factor is as low as 0.301, and the J_{SC} value is obviously lower than other cells. Cells with CE B, C and D exhibit similar J_{SC} values of more than 18 mA/cm^2. Improved performances are achieved by cells with CE B and CE C, of which the fill factor rise to over 0.4, revealing the improvement by the change of graphite flake sizes. The cells with CE D achieve the highest efficiency up to 10.2%, which is only a little lower than the 10.73% efficiency of cells with the expensive Au CE, and the fill factor reaches 0.572. These results show that CEs containing smaller graphite flakes exhibit much better photovoltaic performance compared with CEs consisting of bigger graphite flakes. Moreover, the adding of small CB particles in the CE can further improve the cell performance, especially fill factor. Meanwhile, the over 10% efficiency of HTM-free perovskite cells also clearly demonstrates that our flexible carbon CE is comparable with the expensive Au CE, considering our current technique level of fabricating HTM-free perovskite photoelectrodes [8]. Once better photoelectrodes were used, this type of carbon CE could probably achieve even higher efficiency.

Table 1 Resistivity of different CE samples.

CE sample	graphite flake size	graphite w%	CB w%	resistivity(Ω cm)
A	20 μm	95%	0	0.127
B	3 μm	95%	0	0.677
C	1 μm	95%	0	0.941
D	1 μm	75%	20%	0.802

Table 2 Photovoltaic properties of HTM-free $CH_3NH_3PbI_3/TiO_2$ heterojunction solar cells with different CEs.

CE sample	J_{SC}(mA/cm^2)	V_{OC}(mV)	fill factor	PCE (%)
A	15.29	816.3	0.301	3.76
B	18.30	837.2	0.402	6.16
C	18.85	921.2	0.415	7.21
D	18.73	952.7	0.572	10.20
Au	18.15	910.7	0.649	10.73

The $J-V$ characteristics of HTM-free $CH_3NH_3PbI_3/TiO_2$ heterojunction solar cells with different CEs were evaluated. The

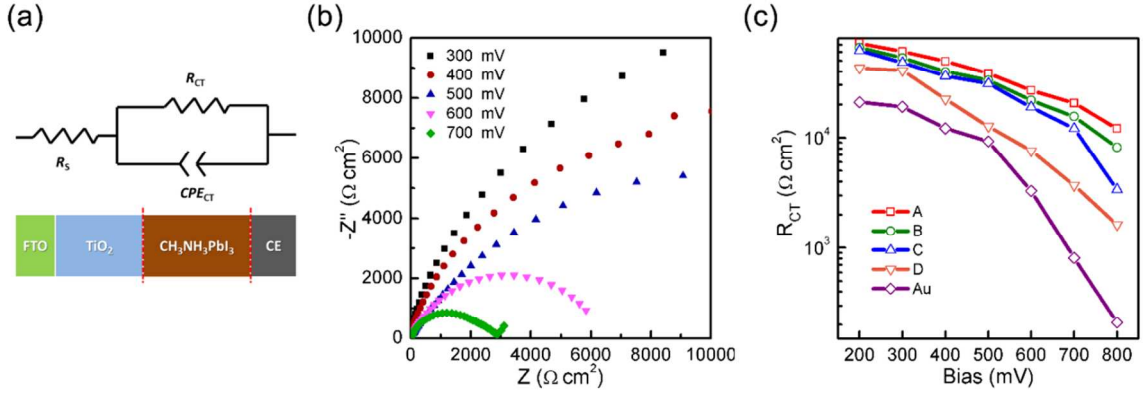

View Article Online
DOI: 10.1039/C4RA09519G

Fig.4 (a) The model for fitting EIS results. R_S is the sheet resistance. R_{CT} is related to the overall charge transfer resistance of the cell, including the contribution of TiO_2/perovskite interface, perovskite layer and perovskite/CE interface. (b) Nyquist plots of the cell with CE D measured at different applied bias. (c) Fitted results of R_{CT} for cells with different CEs.

The electrochemical impedance spectroscopy (EIS) of the cells with both Au CE and our carbon CEs were measured under dark condition at different forward applied bias to investigate the charge transport properties. The Nyquist plots of cells with CE D are presented in Fig. 4(b) as an example. The arc in the Nyquist plots becomes smaller as the applied bias increases. This arc could be related to the overall charge transport in the cell, including the contribution of TiO_2/perovskite interface, perovskite layer and perovskite/CE interface (the perovskite layer and perovskite/CE interface are denoted as "back contact")[23-25]. The simplified model in Fig. 4(a) was used to fit the measured results [26]. The fitted values of R_{CT} for cells with different CEs are shown in Fig. 4(c). Significant differences exists between these cells. Cells with Au CE exhibit the lowest R_{CT} level. For cells with carbon CEs, R_{CT} level increases in order of CE D, C, B and A. This result is quite interesting because the charge transfer resistance at the TiO_2/perovskite interface in these cells should be close to each other, as the photoelectrodes of the cells were fabricated under the same process. Considering that the CE is the only different part in these cells, it can be concluded that the R_{CT} level in perovskite layer is influenced by different CEs. In EIS measurement under dark conditions, the impedances related to TiO_2/perovskite interface and the back contact are series connected. The influence of the back contact can be directly reflected on the measured R_{CT} values. For cells with better back contact, the contribution of the perovskite layer and perovskite/CE interface is smaller, and thus exhibiting smaller R_{CT} values.

The differences in charge transfer resistance contributed by back contact are probably due to the different contact between the perovskite layer and CE. For cells with evaporated Au CE, typically the CE can have quite good contact with the $CH_3NH_3PbI_3$ layer. In this case, charges tend to travel the shortest distance through the $CH_3NH_3PbI_3$ layer, and thus exhibit the lowest charge transport resistance. However, for cells with carbon CE, the situation is quite different. Because of the undulation at the surface of graphite flakes, the graphite flakes and $CH_3NH_3PbI_3$ layer cannot fully contact. The limited contact sites forces the charges to transport through longer distance in the perovskite layer (Fig.5 a), which increases the charge transport resistance. By comparing the R_{CT} levels of cells with CE A, B and C, it can be deduced that the bigger size the graphite flakes have, the fewer contact sites at $CH_3NH_3PbI_3$/CE interface. As for the graphite/CB composite CE (CE D), the lowest R_{CT} level in cells with carbon CEs suggests that the gentler undulation at the surface of smaller graphite flakes, together with the CB particles in the interspace create the most contact sites with the perovskite layer among all the carbon CEs (Fig.5 b).

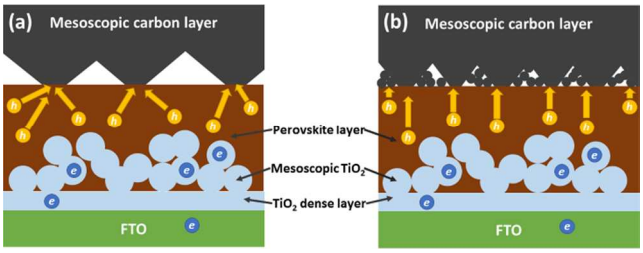

Fig.5 Scheme of charge transfer in HTM-free $CH_3NH_3PbI_3/TiO_2$ heterojunction solar cells with CE consisting of (a) large graphite flakes; (b) composition of smaller graphite flakes and CB particles.

The contact between the CE and perovskite layer affects the cell performance not only by influencing the charge transport resistance in perovskite layer, but may also by possibly altering the charge transfer process at the $CH_3NH_3PbI_3$/CE interface. In dye-sensitized solar cells [27, 28] and quantum-dot sensitized solar cells [29, 30], the surface area of CE is one of the key factors influencing the cell performance [16, 31-33]. CEs with higher surface area have more catalytic sites contacting the electrolyte, and thus exhibit better charge transfer property. In HTM-free perovskite solar cells, holes are transported to the $CH_3NH_3PbI_3$/CE interface, where charge transfer occurs to finish the working cycle of the cell. Similarly, the good contact between the CE and $CH_3NH_3PbI_3$ layer is crucial for the smooth charge transfer process. As the differences of contact sites between different CEs are fierce, it is reasonable to suppose that the charge transfer ability at the $CH_3NH_3PbI_3$/CE interface is affected significantly. For cells with unsatisfactory $CH_3NH_3PbI_3$/CE contact, there may be a bottleneck for the charge transfer process. In this work, the use of smaller graphite flakes and carbon black particles can improve the charge transfer by increasing the contact sites in some degree, which remarkably improve the performance of the cells. Further optimization of the contact between $CH_3NH_3PbI_3$ layer and carbon CE by interface engineering may achieve an even higher efficiency in the future.

Experimental

Materials

PbI_2 (99%) and dimethylformide (DMF, 99.7%) were purchased from Aldrich and Alfar Aesar, respectively. Graphite with different sizes was purchased from Aladdin. The carbon black (acetylene black) was from Denka. All the chemicals were directly used without further purification. CH_3NH_3I was synthesized by following the literature [34].

Substrates for photoelectrode are fluorine-doped tin oxide conducting glass (FTO, Pilkington, thickness: 2.2 mm, sheet resistance 14 $\Omega \cdot square^{-1}$). Before use, FTO glass was firstly washed with mild detergent, rinsed with distilled water for several times and subsequently with ethanol in an ultrasonic bath, finally dried under air stream. The flexible graphite sheets with thickness of 0.2 mm and area density of 0.03 g/cm^2 were cleaned with distilled water, ethanol and then air-dried.

Photoelectrode fabrication

View Article Online
DOI: 10.1039/C4RA09519G

50 nm-thickness TiO_2 compact layers were spin-coated on the FTO, then 450 nm-thickness mesoporous TiO_2 anatase layers were deposited on FTO glass by screen printing method according to the literature [8]. Then, $CH_3NH_3PbI_3$ was deposited on TiO_2 porous films according to a sequential deposition method [4, 26]. That is, 1.2 M PbI_2 in DMF was spin-coated on the TiO_2 film at 2000 rpm for 60 s, then heated at 90ºC for 2 min. After cooling to room temperature, the film was spin-coated with the PbI_2 solution for a second time to increase the amount of PbI_2 and get a relatively smooth film. After dried at 90 °C for another 2 min and cooling down, the films were soaked into CH_3NH_3I isopropanol solution (10 mg/mL) for 120 min. The film color changes from yellow to dark brown. The obtained $CH_3NH_3PbI_3/TiO_2$ films were thoroughly rinsed with isopropanol, dried under air stream, finally heated at 90 °C for 45 min in air on a hotplate. After this procedure, $CH_3NH_3PbI_3$ was evenly formed in the TiO_2 mesoscopic film. Meanwhile, a layer of perovskite capping layer was formed on the TiO_2 mesoporous layer [8], which could separate the TiO_2 layer from the counter electrode.

Counter electrode fabrication

Before the fabrication process, carbon pastes were prepared. Carbon powder was firstly mixed with composite solution of butadiene-styrene rubber and ethyl cellulose in ethyl acetate. The mixture was placed in a ball mill working at 350 rpm for 4 h to form the viscous pastes. A two-step process was then employed to fabricate the counter electrode (Fig. 1). The pastes were first coated on the surface of the as-prepared photoelectrode by the screen-printing technique. Subsequently a piece of graphite paper was tapped and pressed on the carbon paste to be the extraction electrode. The photo of a typical flexible carbon CE is shown in Fig. 3(a). The obtained cell was finally dried at the room temperature for 15 minutes until the solvent was totally volatilized.

Characterization

The cells were irradiated by an Oriel Solar Simulator 91192 under AM 1.5 100 mW/cm^2. Princeton Applied Research, Model 263 A was used to record the *J-V* characteristics of the cells. The thickness of carbon CE films were measured by a profiler (KLA-tencor). The surface morphology of the carbon CEs was observed by a scanning electron microscope (SEM, FEI XL30 S-FEG). The resistance of the carbon films was measured by a four-point probe resistivity measurement system (Four Probes Tech, Guangzhou, China, RTS-9). Electrochemical impedance spectroscopy measurements were performed with an IM6ex electrochemical workstation (ZAHNER). The magnitude of alternative signal was 10 mV.

Conclusions

All-carbon flexible CE has been fabricated for hole-conductor-free organo-metal perovskite solar cells with a low-temperature method. A simple two-step process was employed for the fabrication of the CE. A layer of mesoscopic carbon film was used for the good contact with the perovskite layer, and highly conductive industrial flexible graphite sheet acted as the extraction electrode. It was discovered that the size and morphology of carbon materials played a key role in determining the performance of CEs by influencing the electrical contact at the $CH_3NH_3PbI_3$/CE interface. Perovskite solar cells with CEs consisting of the composition of the smallest graphite flakes and CB particles exhibited the highest efficiency up to 10.2%. The results clearly demonstrate that the performance of our carbon CEs is comparable to expensive Au CE. The low-temperature process and the flexibility of this type of CE show a great potential in developing low-cost and highly efficient flexible perovskite solar cells. Moreover, our study of multiple carbon CEs suggests that the good contact of CE and perovskite layer is the key for high-performance perovskite solar cells with carbon CEs, which can help further improving this type of solar cells in the future.

Acknowledgements

The authors would like to thank the financial support from the NSFC (Nos. 21173260, 51072221 and 91233202), the MOST (973 Project, Nos. 2012CB932903 and 2012CB932904) and the Knowledge Innovation Program of the Chinese Academy of Sciences. The authors also thank Mr. Jiangjian Shi and Mr. Yuzhuan Xu for their helpful discussions.

Notes and references

[a] *Key Laboratory for Renewable Energy, Chinese Academy of Sciences; Beijing Key Laboratory for New Energy Materials and Devices; Institute of Physics, Chinese Academy of Sciences, Beijing, 100190, People's Republic of China.*
** Corresponding author. Email: qbmeng@iphy.ac.cn*

Electronic Supplementary Information (ESI) available. It includes the photovoltaic properties of perovskite solar cells with different graphite/CB ratio, and fitted R_S values in EIS results. See DOI: 10.1039/b000000x/

1. A. Kojima, K. Teshima, Y. Shirai and T. Miyasaka, *J. Am. Chem. Soc.*, 2009, **131**, 6050.
2. M. M. Lee, J. Teuscher, T. Miyasaka, T. N. Murakami and H. J. Snaith, *Science*, 2012, **338**, 643.
3. Q. Chen, H. P. Zhou, Z. R. Hong, S. Luo, H. S. Duan, H. H. Wang, Y. S. Liu, G. Li and Y. Yang, *J. Am. Chem. Soc.*, 2014, **136**, 622.
4. J. Burschka, N. Pellet, S. J. Moon, R. Humphry-Baker, P. Gao, M. K. Nazeeruddin and M. Gratzel, *Nature*, 2013, **499**, 316.
5. J. M. Ball, M. M. Lee, A. Hey and H. J. Snaith, *Energ. Environ. Sci.*, 2013, **6**, 1739.
6. M. Z. Liu, M. B. Johnston and H. J. Snaith, *Nature*, 2013, **501**, 395.
7. O. Malinkiewicz, A. Yella, Y. H. Lee, G. M. Espallargas, M. Graetzel, M. K. Nazeeruddin and H. J. Bolink, *Nat. Photonics.*, 2014, **8**, 128.
8. J. J. Shi, J. Dong, S. T. Lv, Y. Z. Xu, L. F. Zhu, J. Y. Xiao, X. Xu, H. J. Wu, D. M. Li, Y. H. Luo and Q. B. Meng, *Appl. Phys. Lett.*, 2014, **104**, 063901.
9. L. Etgar, P. Gao, Z. S. Xue, Q. Peng, A. K. Chandiran, B. Liu, M. K. Nazeeruddin and M. Gratzel, *J. Am. Chem. Soc.*, 2012, **134**, 17396.
10. W. Abu Laban and L. Etgar, *Energ. Environ. Sci.*, 2013, **6**, 3249.
11. J. Mandelkorn and J. H. Lamneck Jr, *J. Appl. Phys.*, 1973, **44**, 4785.
12. T. Wada, N. Kohara, S. Nishiwaki and T. Negami, *Thin Solid Films*, 2001, **387**, 118.

View Article Online
DOI: 10.1039/C4RA09519G

13. X. M. Fang, T. L. Ma, G. Q. Guan, M. Akiyama, T. Kida and E. Abe, *J. Electroanal. Chem.*, 2004, **570**, 257.
14. T. Leijtens, G. E. Eperon, S. Pathak, A. Abate, M. M. Lee and H. J. Snaith, *Nat. Commun.*, 2013, **4**, 2885.
15. A. Kay and M. Gratzel, *Sol. Energ. Mat. Sol. C.*, 1996, **44**, 99.
16. Z. Huang, X. H. Liu, K. X. Li, D. M. Li, Y. H. Luo, H. Li, W. B. Song, L. Q. Chen and Q. B. Meng, *Electrochem. Commun.*, 2007, **9**, 596.
17. M. X. Wu, X. Lin, T. H. Wang, J. S. Qiu and T. L. Ma, *Energ. Environ. Sci.*, 2011, **4**, 2308.
18. J. K. Chen, K. X. Li, Y. H. Luo, X. Z. Guo, D. M. Li, M. H. Deng, S. Q. Huang and Q. B. Meng, *Carbon*, 2009, **47**, 2704.
19. Q. X. Zhang, Y. D. Zhang, S. Q. Huang, X. M. Huang, Y. H. Luo, Q. B. Meng and D. M. Li, *Electrochem. Commun.*, 2010, **12**, 327.
20. Z. L. Ku, Y. G. Rong, M. Xu, T. F. Liu and H. W. Han, *Sci. Rep.*, 2013, **3**, 3132.
21. Z. Li, S. A. Kulkarni, P. P. Boix, E. Z. Shi, A. Y. Cao, K. W. Fu, S. K. Batabyal, J. Zhang, Q. H. Xiong, L. H. Wong, N. Mathews and S. G. Mhaisalkar, *ACS Nano*, 2014, **8**, 6797.
22. M. Xu, Y. Rong, Z. Ku, A. Mei, T. Liu, L. Zhang, X. Li and H. Han, *J. Mater. Chem. A*, 2014, **2**, 8607.
23. V. Gonzalez-Pedro, E. J. Juarez-Perez, W. S. Arsyad, E. M. Barea, F. Fabregat-Santiago, I. Mora-Sero and J. Bisquert, *Nano Lett.*, 2014, **14**, 888.
24. H. S. Kim, I. Mora-Sero, V. Gonzalez-Pedro, F. Fabregat-Santiago, E. J. Juarez-Perez, N. G. Park and J. Bisquert, *Nat. Commun.*, 2013, **4**, 2242.
25. Z. Li, S. A. Kulkarni, P. P. Boix, E. Shi, A. Cao, K. Fu, S. K. Batabyal, J. Zhang, Q. Xiong, L. H. Wong, N. Mathews and S. G. Mhaisalkar, *ACS Nano*, 2014, **8**, 6797.
26. J. J. Shi, Y. H. Luo, H. Y. Wei, J. H. Luo, J. Dong, S. T. Lv, J. Y. Xiao, Y. Z. Xu, L. F. Zhu, X. Xu, H. J. Wu, D. M. Li and Q. B. Meng, *ACS Appl. Mater. Inter.*, 2014, **6**, 9711.
27. B. Oregan and M. Gratzel, *Nature*, 1991, **353**, 737.
28. A. Hagfeldt, G. Boschloo, L. C. Sun, L. Kloo and H. Pettersson, *Chem. Rev.*, 2010, **110**, 6595.
29. A. J. Nozik, *Physica E*, 2002, **14**, 115.
30. S. Ruhle, M. Shalom and A. Zaban, *Chemphyschem*, 2010, **11**, 2290.
31. Q. H. Li, J. H. Wu, Q. W. Tang, Z. Lan, P. J. Li, J. M. Lin and L. Q. Fan, *Electrochem Commun*, 2008, **10**, 1299.
32. M. X. Wu, X. Lin, Y. D. Wang, L. Wang, W. Guo, D. D. Qu, X. J. Peng, A. Hagfeldt, M. Gratzel and T. L. Ma, *J. Am. Chem. Soc.*, 2012, **134**, 3419.
33. Y. Y. Yang, L. F. Zhu, H. C. Sun, X. M. Huang, Y. H. Luo, D. M. Li and Q. B. Meng, *ACS Appl. Mater. Inter.*, 2012, **4**, 6162.
34. H. S. Kim, C. R. Lee, J. H. Im, K. B. Lee, T. Moehl, A. Marchioro, S. J. Moon, R. Humphry-Baker, J. H. Yum, J. E. Moser, M. Gratzel and N. G. Park, *Sci. Rep.*, 2012, **2**, 591.